AMERICAN SOCIETY FOR MICROBIOLOGY | Antimicrobial Agents and Chemotherapy®

SUSCEPTIBILITY

A Rapid Unraveling of the Activity and Antibiotic Susceptibility of Mycobacteria

A. Mustazzolu,[a] L. Venturelli,[b] S. Dinarelli,[c] K. Brown,[d] R. A. Floto,[d] G. Dietler,[b] L. Fattorini,[a] S. Kasas,[b] M. Girasole,[c] G. Longo[c]

[a]Istituto Superiore di Sanità, Rome, Italy
[b]LPMV–IPHYS, Ecole Polytechnique Fédérale Lausanne, Lausanne, Switzerland
[c]Istituto di Struttura della Materia, Consiglio Nazionale delle Ricerche, Rome, Italy
[d]Molecular Immunity Unit, University of Cambridge, Cambridge, United Kingdom

ABSTRACT The development of antibiotic-resistant bacteria is a worldwide health-related emergency that calls for new tools to study the bacterial metabolism and to obtain fast diagnoses. Indeed, the conventional analysis time scale is too long and affects our ability to fight infections. Slowly growing bacteria represent a bigger challenge, since their analysis may require up to months. Among these bacteria, *Mycobacterium tuberculosis*, the causative agent of tuberculosis, has caused more than 10 million new cases and 1.7 million deaths in 2016 only. We employed a particularly powerful nanomechanical oscillator, the nanomotion sensor, to characterize rapidly and in real time tuberculous and nontuberculous bacterial species, *Mycobacterium bovis* bacillus Calmette-Guérin and *Mycobacterium abscessus*, respectively, exposed to different antibiotics. Here, we show how high-speed and high-sensitivity detectors, the nanomotion sensors, can provide a rapid and reliable analysis of different mycobacterial species, obtaining qualitative and quantitative information on their responses to different drugs. This is the first application of the technique to tackle the urgent medical issue of mycobacterial infections, evaluating the dynamic response of bacteria to different antimicrobial families and the role of the replication rate in the resulting nanomotion pattern. In addition to a fast analysis, which could massively benefit patients and the overall health care system, we investigated the real-time responses of the bacteria to extract unique information on the bacterial mechanisms triggered in response to antibacterial pressure, with consequences both at the clinical level and at the microbiological level.

KEYWORDS antibiotic response, collective movements, fast characterization, metabolic activity, mycobacteria, nanomotion sensor, susceptibility

Providing fast and reliable antibiotic susceptibility data, which enables the initiation of prompt and appropriate therapy schedules, is a main task of the clinical laboratory. While molecular techniques (i.e., matrix-assisted laser desorption ionization–time of flight mass spectrometry [MALDI-TOF MS] or PCR-based gene amplification) (1, 2) have radically changed the time frame for Gram-positive and -negative bacterial identification (ID), most of the current methods for antimicrobial susceptibility testing (AST) are based on fluorescence staining or phenotypic assays (1, 3) which may require days, or even weeks, depending on the bacterial species. In a conventional clinical workflow, the sample (e.g., blood, spinal fluid, urine, feces, and nasal or throat swabs) is harvested from patients, streaked on agar nutrient medium, and, after 12 to 24 h of incubation, transferred for further analysis. This unavoidable culture step results in the isolation of microorganisms in liquid cultures containing up to 10^8 to 10^9 CFU/ml (4). ID and culture-based AST are performed after this incubation time and can last more than 24 h (5). Similar protocols are commonly used for slowly growing bacteria such as

Citation Mustazzolu A, Venturelli L, Dinarelli S, Brown K, Floto RA, Dietler G, Fattorini L, Kasas S, Girasole M, Longo G. 2019. A rapid unraveling of the activity and antibiotic susceptibility of mycobacteria. Antimicrob Agents Chemother 63:e02194-18. https://doi.org/10.1128/AAC.02194-18.

Address correspondence to G. Longo, longo@ism.cnr.it.

A.M. and L.V. contributed equally to the work.

Received 17 October 2018
Returned for modification 16 November 2018
Accepted 14 December 2018
Accepted manuscript posted online 2 January 2019
Published 26 February 2019

mycobacteria, but in these cases, the incubation time can be longer than a week (e.g., in the MGIT 960 system), and more than one month may be required to obtain ID and AST (5). This long time frame, under the pressure of life-threatening infections, often results in imprudent use or misuse of antibiotics. Early appropriate therapy will significantly reduce the spread of pathogenic bacteria into the population. This will lead to a higher patient survival rate, lower distress, and an optimized use of the limited resources of health care systems (6, 7).

Many options are emerging to achieve a rapid, accurate, and cost-effective pathogen characterization of bacterial responses to drugs, ranging from molecular to rapid phenotypic techniques to plasmonic single-cell assays (8–11). The conventional AST molecular techniques rely mainly on the determination of the genetic fingerprint associated with resistance to a specific antibiotic, including real-time PCR (RT-PCR), DNA microarrays, next-generation sequencing (NGS), cell lysis-based approaches, whole-genome sequencing, and MALDI-TOF MS (12–16). Even though the aforementioned techniques can provide fast and high-throughput results, they still present profound drawbacks. For instance, their outcome is strongly dependent on specific drug target genes, which can only be indicative of the actual antibiotic resistance, leaving a large gap for drug phenotypic response.

Novel single-cell techniques have gained importance in the last decade, in particular, for cancer-related applications. Nevertheless, the analysis of bacterial susceptibility requires the concurrent evaluation of hundreds or thousands of bacteria to assess response at the population level. Thus, their application is mostly limited to the research laboratory, and their low throughput hinders their transition to a clinical susceptibility test.

Most commercial phenotypic assays rely on bacterial replication to deliver a correct AST, and the time scale for antibiogram determination may range from days for rapidly replicating bacteria to weeks or months for slowly growing and fastidious germs. To shorten turnaround times and costs, several automated systems are now available, including, for instance, MicroScan WalkAway (Beckman Coulter), BD Phoenix (Dickinson Becton), Vitek-2 (bioMérieux), and SIDECAR (Alifax) (17, 18). The outcome is a relatively rapid susceptible/resistant response which is available to the clinician as soon as the second day from the first examination of the sample, with large advantages for treatment but still too long for severe infections (e.g., meningitis, sepsis) (1, 3). In addition, most of these techniques provide no clue on the particular drug effect or on the counter mechanisms employed by bacteria to react to antibiotic compounds.

Among the alternatives to conventional microbiological assays, small and extremely sensitive nanomechanical oscillators (19) stand out as very promising candidates (8, 9, 20, 21). At first, such devices were employed in atomic force microscopes (AFMs) to study dynamic behavior in cells (22) or proteins (23, 24). Nowadays, they are increasingly used for the detection of very small masses (25) or for nanostress sensing in molecular biology (26), and their sensitivity and versatility are exploited in lab-on-a-chip devices to measure biomolecular interactions (27) or mass variations in biological systems, including bacteria (28, 29). Two major factors limit most of the available nanomechanical systems: (i) they require air or vacuum conditions for the measurements, and (ii) they need bacteria to replicate directly on the sensors and to determine cell viability through mass change or local stress alterations. This reflects on the time required to perform the analysis and on the range of information that can be obtained, based on life or death assessments.

Very recently, we introduced a new way of exploiting the capabilities of cantilever nanosensors: the nanomotion sensor (NMS) (30, 31). By exploiting the intimate link between life and motion, measuring the fluctuations of flexible cantilevers that act as a solid support for microorganisms, we can monitor in real time the metabolism of living organisms (32). The sensor's fluctuations strongly depend on the microorganisms' metabolic activities, which combine energy consumption, cell vibration, and movement. The sensitivity of the technique enables the detection of energy consumption of a few ATP molecules, as demonstrated in previous works using finite elements mod-

eling or studying conformational changes in quaternary protein structures (31, 33). Thus, the NMS can been used to evaluate the fluctuations of a very limited number of viable specimens (single mammalian cells or tens of bacteria) (32, 34–37).

By measuring the fluctuations as a function of time and of external conditions, the NMS delivers unique insight on a microorganism's response to environmental, chemical, or physical stimuli (32). The amplitude and the low frequency of these fluctuations (<1 kHz) help circumvent the major limitations of current nanomechanical sensors: the NMS can be used under various conditions (i.e., in buffer solutions or growth medium), and the viable specimens are attached to both sides of the sensor, reducing the complexity and cost of each experiment. In addition, due to the time resolution of the NMS, these experiments enable investigations in real time and with sensitivity in the angstrom-to-micron range (33) of the evolving metabolism of the adsorbed bacteria, long before a single replication (30, 31). This suggests that the analysis time scales are only marginally dependent on bacterial duplication rates, as demonstrated by studying *Bordetella pertussis*, which replicates in 48 h (38). In addition, the sensitivity of these sensors enables the extraction of a measurable signal from groups of fewer than 100 bacterial cells, leading to a drastic reduction in incubation times. Overall, the outcome is a quantitative evaluation of the real bacterial response to the applied stimuli, on a time scale (hours) comparable to that of the fastest molecular analyses (39). Furthermore, the real-time monitoring of a nanomotion susceptibility test (N-AST) reveals a different kind of information on the bacterial behavior compared to that from conventional phenotypic and genetic studies, with the potential to improve therapeutic interventions, which are paramount for clinical decisions, and, hopefully, therapeutic outcomes, as demonstrated in previous works on rapidly growing bacteria (40). For this reason, coupling the NMS with other conventional techniques could help to better unravel which molecular processes arise to account for specific observed motion change behavior.

RESULTS

We exploited the capabilities of the NMS to study slowly growing *Mycobacterium bovis* bacillus Calmette-Guérin (BCG) and the fast growing nontuberculous mycobacterium (NTM) *Mycobacterium abscessus* (41). In particular, the former species belongs to the *Mycobacterium tuberculosis* complex (MTC), which includes *M. tuberculosis* and *M. africanum*, representing a growing medical emergency in both developing and developed regions (42). By studying their nanomotion, we characterized the interaction between these two species and three antibacterial drugs and were able to determine in a matter of hours their susceptibility, calculating their MICs and minimum bactericidal concentrations (MBCs). Furthermore, we exploited the real-time analysis of the NMS to evaluate the peculiar responses of these bacteria to the different antibacterial agents. We chose to work with a relatively large number of bacteria on the sensor (approximately between 100 and 1,000 cells) to ensure a good population-level analysis of the susceptibility and to average out the possible presence of outliers or single naturally resistant microorganisms.

In preliminary experiments, we determined whether NMS preparation protocols influenced the viability of BCG and *M. abscessus* in the MGIT medium. Overall, we kept the bacteria for at least 200 min in the analysis chamber by monitoring the oscillations over time. As shown in Fig. 1, the variance of the nanomotion signals remained constant over time, indicating that the bacteria were viable for the entire control experiment.

BCG. We performed a series of experiments involving the exposure of BCG to rifampin (RIF) or isoniazid (INH), two first line antituberculosis (anti-TB) drugs inhibiting the DNA-dependent RNA polymerase and specific enzymes implicated in cell wall synthesis, respectively (42, 43). We selected this species because it belongs to the MTC, is not dangerous to humans, and can be safely handled in a biosafety level 2 laboratory, constituting a safe NMS testing ground for the study of more dangerous mycobacteria, including *M. tuberculosis*.

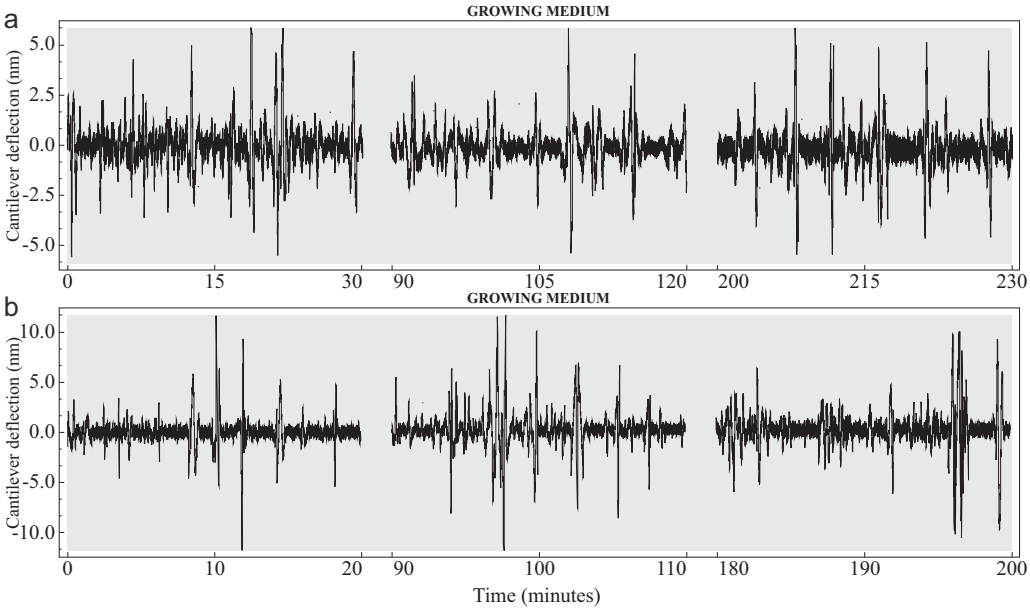

FIG 1 Control experiments involving BCG and *M. abscessus*. Typical data patterns (performed minimally in triplicates) of BCG (a) and *M. abscessus* (b) in MGIT medium. The fluctuations are present for more than 200 min.

When exposed to bactericidal doses of these agents, the BCG produced a sharp reduction of the sensor's fluctuations, underlining the drug's activity. In a typical experiment, the outcome of the exposure to a bactericidal dose of INH (2 μg/ml) was determined in less than 30 min (Fig. 2). On the other hand, after exposure to a high dose of RIF (0.7 μg/ml) (Fig. 3), we observed a reduction in the sensor's movement, demonstrating a slower bactericidal effect and confirming bacterial death, which required almost 2 h.

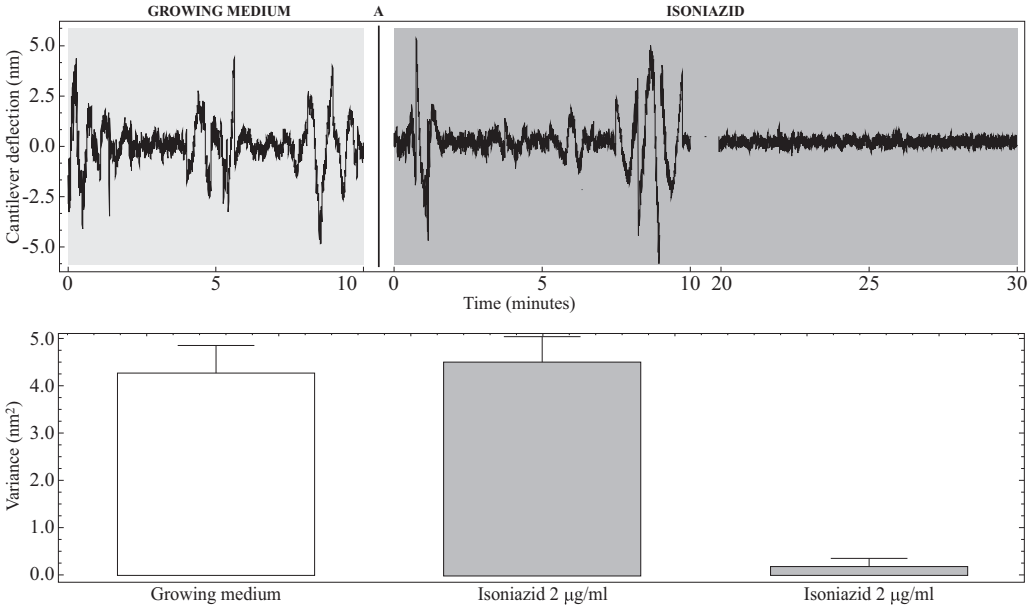

FIG 2 Nanomotion experiments on BCG exposed to an over-MIC dose of INH. (Top) Typical 10-min segments of the sensor's fluctuations before the exposure to INH (left), immediately after the exposure to INH at 2 μg/ml (center), and 20 min after the exposure to INH, when the movement reduction has stabilized. (Bottom) Histogram of the corresponding variance of the fluctuations. The graph is representative of minimally 5 independent experiments which produced similar results. The error bars represent SDs of the fluctuations during the corresponding 10-min time periods.

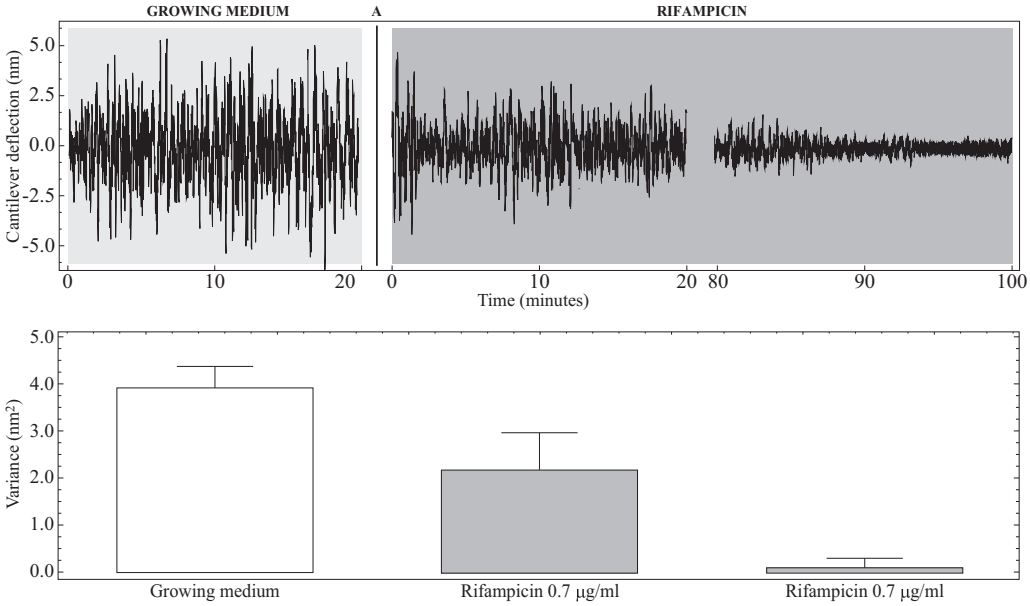

FIG 3 Nanomotion experiments on BCG exposed to an over-MIC dose of RIF. (Top) Typical 20-min segments of the sensor's fluctuations before the exposure to RIF (left), immediately after the exposure to RIF at 0.7 μg/ml (center), and 80 min after the exposure to RIF, when the movement reduction has stabilized. (Bottom) Histogram of the corresponding variance of the fluctuations. The graph is representative of 3 independent experiments which produced similar results. The error bars represent SDs of the fluctuations during the corresponding 20-min time periods.

The subsequent step in the analysis of the response of BCG to these antibacterial agents consisted of a series of dose dependence experiments. The results, summarized in Fig. 4a for INH and in Fig. 4b for RIF, indicate for each experiment the relative reduction of the nanomotion fluctuations. In both cases, the linear fit of the sigmoid curve was used to determine the MIC and MBC values. The obtained values were an MIC of 0.09 ± 0.03 μg/ml and an MBC of 0.17 ± 0.03 μg/ml for INH and an MIC of 0.15 ± 0.07 μg/ml and an MBC of 0.4 ± 0.07 μg/ml for RIF. The MICs of BCG Pasteur determined by NMS differed by approximately 1-fold dilution from those determined by conventional proportion methods (0.2 versus 0.09 μg/ml for INH, and 0.063 versus 0.15 μg/ml for RIF, respectively) (44–46). Such discrepancy between the conventionally

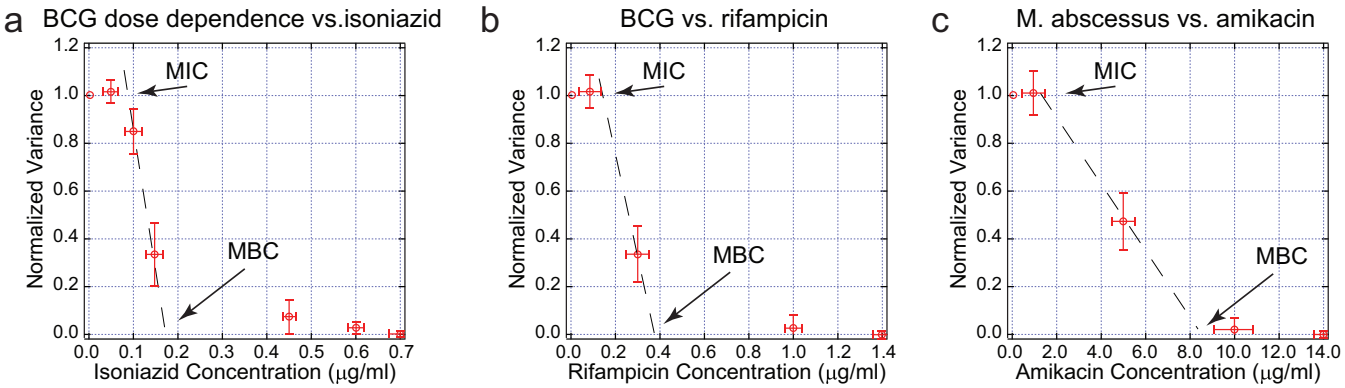

FIG 4 Dose dependence experiments. (a) Normalized variance calculated from the deflections collected by exposing BCG to different INH concentrations. (b) Normalized variance calculated from the deflections collected by exposing BCG to different RIF concentrations. (c) Normalized variance calculated from the deflections collected by exposing *M. abscessus* to different AK concentrations. The concentration values can be well fitted with a sigmoid function, which is comparable with the antibiogram plots obtained using conventional microbiological techniques. The MIC and MBC toward the bacterial species can be obtained by calculating the tangents of the sigmoid fits at half height (black dashed lines). Each data point represents the average from a minimum of 3 independent experiments performed using the same drug concentration. The error bars represent the variability of the different experiments performed at the same concentration. In each graph, the experiments involving sub-MIC drug concentrations are represented as a single data point, which summarizes all these experiments.

measured MIC and the N-AST is something that has been also highlighted in previous experiments involving rapidly growing bacteria (31, 39). This difference can be attributed to many factors, such as growth conditions, measurement geometry, or temperature. It must be noted that conventional and NMS assays monitor different metabolic parameters. In most conventional analyses, the MIC is identified by the bacterial ability to replicate, while for the NMS, this concentration is associated with the reduction of the sensor's fluctuations, associated with alterations in the bacterial membrane elasticity (36, 37) or to their internal metabolic activity. Indeed, while the information is similar, the concentration at which one or the other phenomenon occurs can be different.

In addition to these quantitative susceptibility results, performing a real-time analysis on antibiotics susceptibility enabled us to evaluate how the drug pressure influenced the investigated microorganisms, including their peculiar response patterns and typical time scales. For instance, INH exposure, even if using sub-MICs, caused an immediate response of BCG, which was registered as a fluctuation intensity increase that lasted 10 to 15 min before a rapid decay of the movements. After a few tens of minutes, if the concentration was not bactericidal (i.e., 0.025 μg/ml) (Fig. 5a), the variance of the fluctuations recovered and their intensity returned to values comparable to those measured before the antibiotic injection. This entire response pattern did not last more than 20 min. On the other hand, if the drug concentration was higher than the MBC (e.g., 1 μg/ml) (Fig. 6), the response was more complex. After an initial rise in the oscillations, the movements rapidly decreased to lower values for up to 25 min, followed by a few seconds of wide fluctuations. This biphasic pattern repeated itself several times for more than 1 h, until the fluctuations stabilized to low values, indicating the death of the BCG. A possible interpretation of this pattern is related to BCG clumping: these bacteria exploit their waxy coating to form cell aggregates that do not completely dissolve during sample preparation procedures. In such clumps, external bacteria are expected to be metabolically more active than internal ones, partially shielding them from some environmental attacks. In this view, the bactericidal antibiotics could kill, at first, the cells of the external layer, and then the internal bacteria would be activated, resulting in the movement-stasis pattern we observed and measured. Clumping is an already known defense mechanism in microbiology and can be found in many different species, such as in *Candida albicans*, in self-aggregation in *Escherichia coli*, or in flocculation in *Saccharomyces cerevisiae* (47–50), but it has never been reported in this way for BCG.

While we identified these peculiar movements in INH-exposed BCG, these were never seen in RIF experiments (Fig. 5b), suggesting that this behavior is strictly dependent on the response mechanism of BCG to INH. Indeed, the response against 0.07 μg/ml of RIF did not involve a strong initial reaction to the drug, with fluctuations lasting from 1 to 2 h. In some cases, within minutes of drug exposure, we measured a temporary reduction of movements, which lasted up to 30 min, followed by full recovery of the nanomotion fluctuations. Furthermore, in RIF-exposed BCG, we never identified the oscillating patterns seen for INH. A possible interpretation of the different reported behaviors with respect to the two different drugs might rely on their different time scales for the effect. While INH affects cell wall synthesis, its effect is quite fast, and the shielding of the clumping might produce a visible transitional oscillation. On the other hand, since RIF targets RNA polymerase, consequently blocking protein translation, its longer time scale might cover the aforementioned effect.

***M. abscessus*.** To investigate the response of drugs against *M. abscessus*, we used the protein synthesis inhibitor amikacin (AK), because this organism is known to be resistant to INH and RIF. In the presence of a bactericidal concentration of the drug (10 μg/ml) (Fig. 7a), *M. abscessus* did not show an immediate response, with no alterations of the fluctuations for the first 30 min, followed by a sharp decrease of the movements between 50 and 70 min, after which the fluctuations did not recover. When nonbactericidal doses were used (1 μg/ml) (Fig. 7b), a lag phase of approximately 10 to

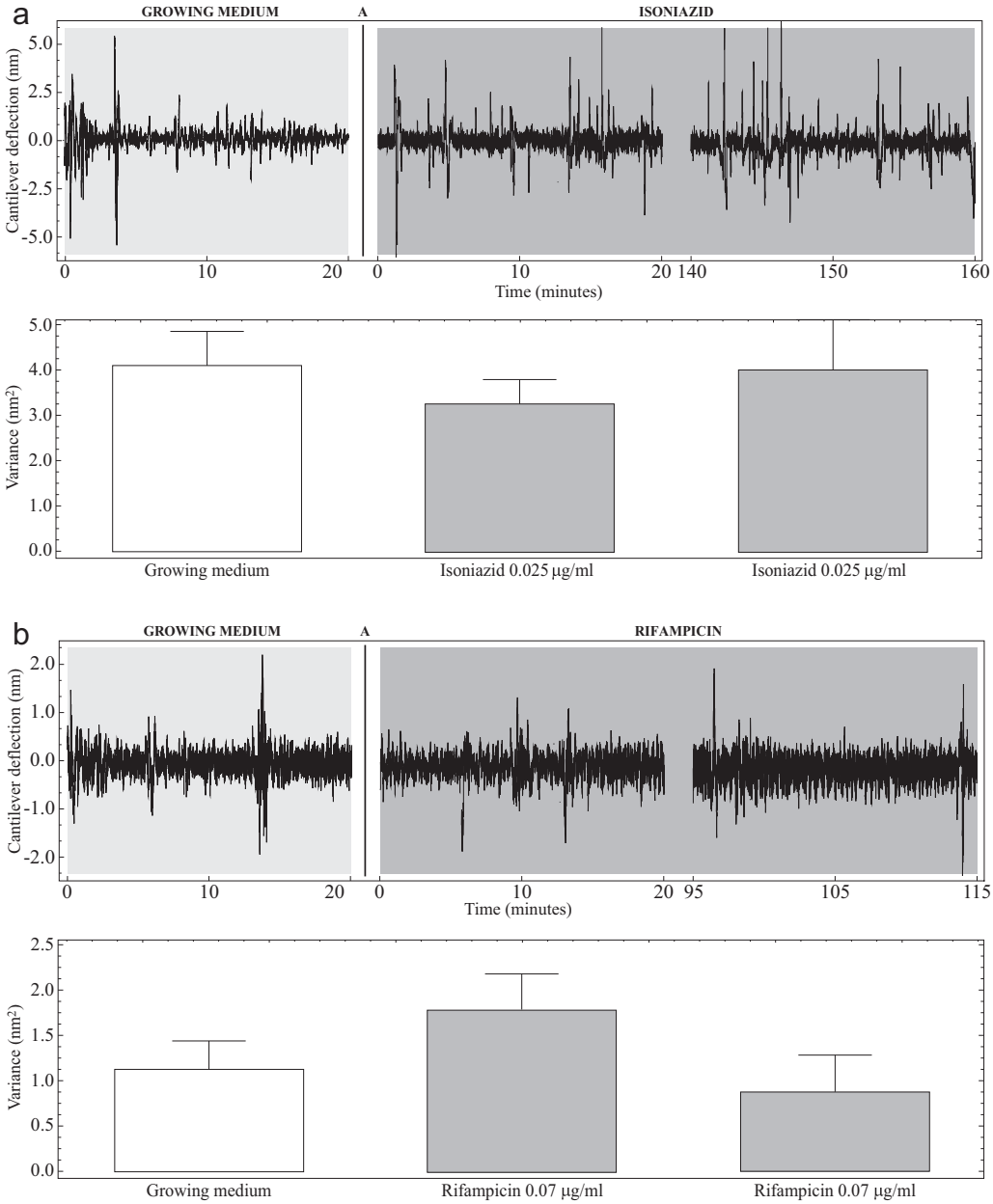

FIG 5 Nanomotion experiments on BCG exposed to a sub-MIC doses of INH and RIF. (a, top) Typical 20-min segments of the sensor's fluctuations before the exposure to INH (left), immediately after the exposure to INH at 0.025 μg/ml (center), and 140 min after the exposure to INH, when the movement has stabilized. (Bottom) Histogram of the corresponding variance of the fluctuations. (b, top) Typical 20-min segments of the sensor's fluctuations before the exposure to RIF (left), immediately after the exposure to RIF at 0.07 μg/ml (center), and 95 min after the exposure to RIF, when the movement has stabilized. (Bottom) Histogram of the corresponding variance of the fluctuations. Each graph is representative of minimally 3 independent experiments which produced similar results. The error bars represent SDs of the fluctuations during the corresponding 20-min time periods.

25 min was observed, followed by a full recovery of the nanomotion signal. This trend is in line with the NMS response of *Staphylococcus aureus* exposed to cefoxitin (31) or *E. coli* to ceftriaxone (39). It is worth noting that the response time of *M. abscessus* to AK (50 to 70 min) is longer than in the BCG INH case (20 to 30 min) and comparable with the BCG RIF time scales (80 to 100 min). This can be attributed to the different mechanisms of action of AK compared to that of INH. Indeed, INH inhibits cell wall synthesis and is expected to have a more rapid effect than RIF and AK, which inhibit protein synthesis. Remarkably, the response times of the BCG and *M. abscessus* are

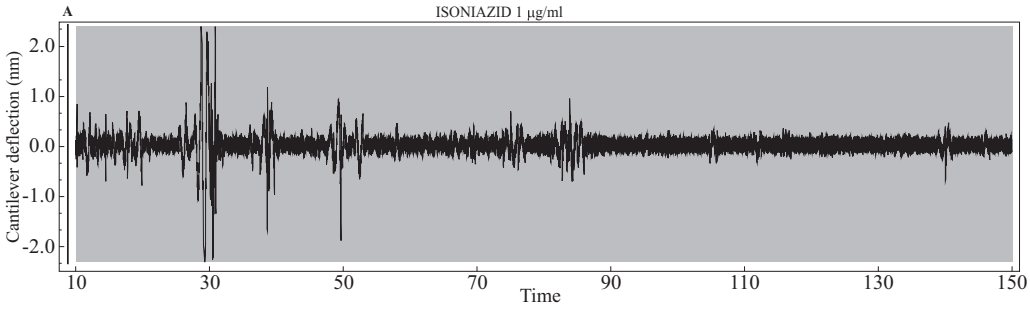

FIG 6 Time-resolved analysis of the BCG response to INH. Typical data pattern of the response of BCG to a bactericidal dose of INH (1 μg/ml). Over a 140-min period, the fluctuations increase and decrease in amplitude, highlighting the bacterial response to the antibiotic pressure. The graph is representative of 3 independent experiments in which this feature was evidenced.

similar to the typical time scales of the experiments involving rapidly replicating bacteria (between 15 and 60 min for both *E. coli* and *S. aureus* [31, 39]). This clearly demonstrates the nanomotion sensor's independence of the replication rate of the specimens under investigation. Furthermore, it also depicts the range of interesting new information that the technique can provide.

As conducted for BCG, we performed a series of dose dependence measurements to obtain quantitative susceptibility results for *M. abscessus* exposed to AK (Fig. 4c). The linear fit for the sigmoid curve indicated a MIC of 1.7 ± 0.6 μg/ml and a MBC of 7.8 ± 0.6 μg/ml. These concentrations are in good agreement (within one dilution) with those present in the literature for this reference *M. abscessus* strain (3.1 versus 1.7 μg/ml) (51, 52).

DISCUSSION

M. tuberculosis and NTM are the causative agents of extremely dangerous infections, such as TB, which caused 10.4 million new cases and 1.7 million deaths in developing and industrialized countries in 2016 (53). A fast diagnosis of these bacteria will enable a more specific tailored treatment that is more effective and better tolerated by the patient and less likely to produce relapses. An early diagnosis of infections from slowly growing bacteria could be lifesaving and could significantly reduce the spread of harmful pathogens into the population, leading to a higher survival rate, lower distress, and an improved use of the limited resources of the health care system (54, 55).

This work shows how the NMS can be used to obtain a rapid and reliable investigation of the MTC and NTM, with possible impacts in the early clinical and diagnostics fields. Indeed, while the clinical application of the NMS has already been demonstrated on *E. coli* (39), its importance to the study of slowly growing germs can be safely suggested. In addition, the speed of the nanomotion analyses enables a rapid screening of innovative molecules and antitubercular agents to accelerate and reduce the costs for drug discovery and drug development (56, 57). Furthermore, the NMS highlights the specific behavior of slowly growing bacteria during antibiotic treatment, evidencing cooperative vibrations and activity reduction, which could not be determined using other phenotypic techniques. This provides better overviews of the metabolism of slowly growing bacteria in models more closely mimicking *in vivo* microenvironments and of their dynamic responses to external stimuli, which are of great importance in medical and pharmacological TB research. These results illustrate how N-AST can become a reliable and rapid investigation tool for slowly growing bacterial species, providing also new insight into the behavior of these bacteria during antibiotic treatment.

The possible combination of NMS and molecular biology assays would deliver thorough comprehension of the bacterial resistance mechanisms, which could provide invaluable information to produce newer more-targeted drugs and antimycobacterial agents to fight some of the deadlier diseases of our times.

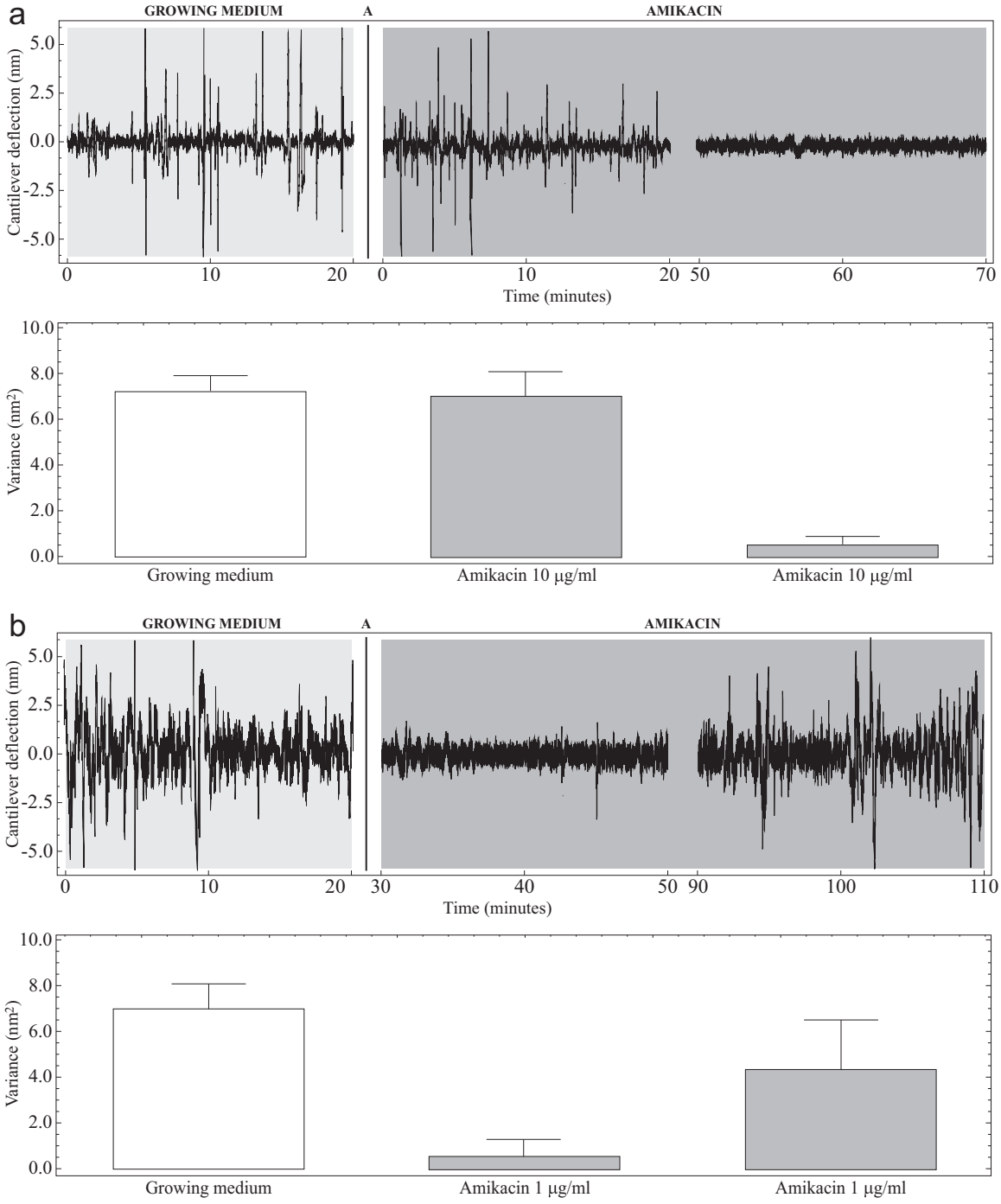

FIG 7 Nanomotion experiments on *M. abscessus* exposed to AK. (a, top) Typical 20-min segments of the sensor's fluctuations exposed to an over-MIC dose of AK before the exposure to AK (left), immediately after the exposure to AK at 10 μg/ml (center), and 50 min after the exposure to AK, when the movement has stabilized. (Bottom) Histogram of the corresponding variance of the fluctuations. (b, top) Typical 20-min segments of the sensor's fluctuations exposed to a sub-MIC dose of AK before the exposure to AK (left), 30 min after the exposure to AK at 1 μg/ml (center), and 90 min after the exposure to AK, when the movement has recovered and stabilized. (Bottom) Histogram of the corresponding variance of the fluctuations. Each graph is representative of at least 3 independent experiments which produced similar results. The error bars represent SDs of the fluctuations during the corresponding 20-min time periods.

MATERIALS AND METHODS

Substrates, enzymes, and reagents. Chemicals, phosphate-buffered saline (PBS), glutaraldehyde, and the antibiotics rifampin (RIF), isoniazid (INH), and amikacin (AK), all of analytical grade, were obtained from Sigma-Aldrich (St. Louis, MO). MGIT 960 (MGIT) tubes (Becton, Dickinson Microbiology Systems, Sparks, MD) were used to obtain the bacterial culture medium.

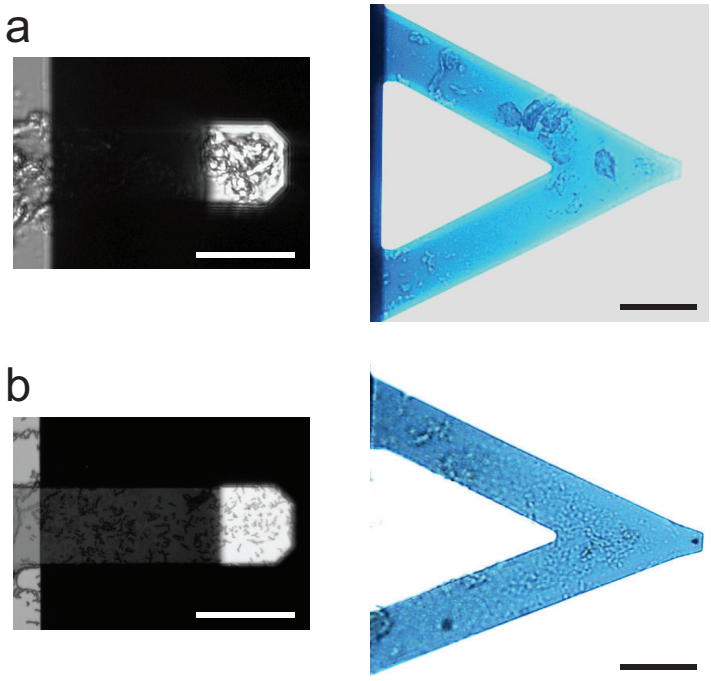

FIG 8 Optical images of bacterium-bearing sensors. Typical optical images of rectangular (left panels) and triangular sensors (right panels) bearing BCG (a) and *M. abscessus* (b). The optical images show the BCG clumping. Scale bars, 50 μm.

Bacterial preparation and isolation. *Mycobacterium bovis* BCG (ATCC 27291 [Pasteur strain]) cells frozen at −70°C were thawed and grown in Löwenstein Jensen slants at 37°C for 3 weeks. A few colonies were transferred to tubes containing 500 μl of MGIT medium. Since the BCG tends to form clumps that are difficult to disaggregate, the tubes were vortexed to ensure that any large bacterial clump was dissolved or reduced before transferring the bacterium-rich medium to the nanomotion experiments. As shown in Fig. 8, small BCG clumps were still present on the sensors. The MIC of BCG Pasteur was determined using the proportion method. The characterizations showed that, in good agreement with the values present in the literature, the MICs were 0.2 μg/ml for INH (45) and 0.063 μg/ml for RIF (46), with an uncertainty of one dilution.

Mycobacterium abscessus (ATCC 19977) cells frozen at −70°C were thawed, and the specimens were grown in MGIT medium at 37°C for 3 days under continuous agitation. One milliliter of the bacterium-rich medium was centrifuged (5,000 rpm for 5 min), and the pellet was resuspended in PBS and transferred directly to nanomotion experiments. The susceptibility values present in the literature for ATCC 19977 toward amikacin detail a MIC of 3.1 μg/ml, with an uncertainty of one dilution (52).

Nanomotion experiments. The nanoscale movements of the microorganisms induced dynamic deflections of the NMS, which were monitored in real time using the laser-based signal transduction typically used in most AFMs. These fluctuations were plotted as a time-dependent chart of the vertical movements of the sensor, which appeared as a colored noise signal with superposition of a large number of vibrations. Overall, a typical experiment lasted more than 2 h, divided into data chunks of at least 30 min. The control experiments were carried out for at least 4 h. In each experiment, the sensors were followed in real time using optical cameras.

A commercial Nanowizard III microscope (JPK Instruments, Berlin, Germany) and custom homemade devices developed in the Laboratories of Living Matter Physics at the EPFL (LPMV-EPFL) were used. The sensors chosen for the JPK experiments were the ONP-10 tipless AFM cantilevers from Bruker (Bruker Nano Inc., MA, USA). For the homemade devices, SD-qp-CONT tipless cantilevers (NanoandMore GmbH, Germany) were employed. For all experiments, sensors with spring constants in the range of 0.08 $\pm$ 0.03 N/m were used, which demonstrated good sensitivity coupled with geometrical properties that ensured space for an adequate number of bacteria (as controlled through optical images throughout each experiment). The data from the Nanowizard III microscope were collected using the JPK software with a 10-kHz acquisition rate, while the data from the experiments on the custom devices were collected using a USB-4431 DAQ card (National Instruments, USA) with a 20-kHz acquisition rate. Remarkably, as a demonstration of the solidity of the analysis technique, the results obtained with the two different instrumentations were compared, showing similar sensitivities and noise levels.

To enhance bacterial adhesion, as established and detailed in many previous works, the sensors were chemically treated. In the literature, there are examples where fibronectin, poly-lysine, polyethylene imine, (3-aminopropyl)triethoxysilane (APTES), glutaraldehyde, concanavalin, or even collagen was used for this purpose (15, 40, 58–61). In comparison with the specimens analyzed in some previous works (62),

the thick, hydrophobic, and waxy cell walls of mycobacteria required new immobilization strategies and the use of specific culture media and drugs. In the present work, the sensors were exposed to 0.5% glutaraldehyde for 15 min, followed by rinsing in ultrapure water and air drying. This immobilization protocol enabled the mycobacteria to adhere to the sensors with little influence on their metabolic activity (as demonstrated by the control experiments depicted in Fig. 1).

Both instruments were equipped with closed custom analysis chambers made of plastic or polydimethylsiloxane (PDMS), which enabled experiments in liquids to be performed with very little noise from changing the medium (63).

For the subsequent immobilization of the living bacteria on the sensors, a protocol that ensured marked adhesion of the cells on the sensors was used. Since the growth medium often contained complex molecules that might passivate the chemical functionalization on the sensor, aliquots of MGIT-containing bacteria were washed twice in PBS (by centrifuging cells at 3,000 $\times$ *g* for 5 min, and resuspending the pellet in 100 μl of PBS to a final optical density [OD] that ranged from 10^6 to 10^8 CFU). To let the bacteria adhere to the sensor, a droplet (typically 20 μl) of the bacterium-rich PBS was deposited on the sensor and incubated at room temperature for approximately 15 min. This protocol results in a roughly uniform distribution of bacteria on the sensor surface, with inherent variability in their numbers and spatial distribution. Thereafter, the sensor was mounted on the holder and inserted into the analysis chamber carrying 2 ml of MGIT medium for the analyses. As shown in the optical images of the sensors during the experiments (Fig. 8), approximately 100 to 1,000 cells adhered to the NMS; more complex procedures must be carried out to obtain a quantitative determination (31). It is worth highlighting that the immobilization protocol produces a variability in the absolute value of the oscillations, which are different for each experiment, but the strong attachment ensures that the number and position of the bacteria are well preserved throughout each single analysis.

As detailed in previous works, to generate dose dependence curves, several parallel experiments in which the bacteria were exposed to different concentrations of antibiotic drugs were compared. For these graphs, the relative reduction of the fluctuations was compared to the maximum variance measured before the exposure to the chosen drug concentration. This enabled a comparative measure of the bacterial response to be defined as well as comparisons and averaging of the many experiments performed. Each experiment was performed at least in triplicates, lasted at least 2 h, and comprised three steps: (i) preparation of viable bacteria in medium (BCG or *M. abscessus* in MGIT medium), (ii) exposure to the desired drug concentration (INH, RIF, or AK), and (iii) exposure to a high bactericidal drug concentration (31). The concentration dependence curve was then fitted with a sigmoid curve interpolation, containing information similar to that in a conventional antibiogram. By performing a linear fit of the central part of the sigmoid, two concentration values were calculated, which are associated with the MIC (the drug concentration that inhibits visible bacterial growth) and the minimum bactericidal concentration (MBC; the concentration that ensures the death of 99.9% of the bacteria) (31). New AST assays intended as substitutes of conventional microbiological procedures should provide these two concentrations, and this is one of the main advantages of phenotypic assays compared to faster molecular counterparts. Indeed, just as for the conventional values, at drug concentrations below the nanomotion-obtained MIC (NM-MIC), the fluctuations of the cantilever are largely unaffected, while at values higher than the NM-MBC, the movements are largely reduced.

Statistical analysis. The nanomotion data are presented as acquired, with a simple linear fit to remove any long-term drift from the traces. The variance calculations are presented as histograms and standard deviations (SDs) calculated from the corresponding fluctuations over the corresponding raw data, but the trends are indicative of at least three independent sample preparations.

Each data point of the dose dependence graphs was obtained from minimally three independent experiments, and the graphs were drawn according to procedures detailed elsewhere (31). The error bars represent the variability of the different experiments performed at each concentration.

Data availability. All the presented data are available upon reasonable request. Fig. 1, 2, 3, 5, 6, and 7 present raw data. All data collection and analysis were performed using custom Labview code, which is freely available upon reasonable request.

ACKNOWLEDGMENTS

We thank A. Kalauzi and K. Radotic from the Center for Multidisciplinary Studies, Laboratory of Biophysics, University of Belgrade, for their help with the nanomotion data processing.

G.L., S.D., and M.G. were funded by the Consiglio Nazionale delle Ricerche, short-term mobility program no. CUP B53C17001680005.

S.K., G.D., and L.V. were funded by the Swiss National Grants 200021-144321 and 407240_167137, the Gebert Rüf Stiftung GRS-024/14, and NASA NNH16ZDA001N-CLDTCH.

No funding bodies had any role in study design, data collection and analysis, decision to publish, or preparation of the manuscript.

G.L., A.M., and L.V. performed the nanomotion experiments; S.K. and G.D. provided the nanomotion sensor infrastructure; G.L., S.K., and G.D. developed and optimized the methodology; G.L. and L.V. developed the software; A.M. and L.F. provided and characterized the BCG; K.B. and R.A.F. provided and characterized the *M. abscessus*; G.L.,

L.V., S.D., and M.G. performed the data analysis; G.L., L.V., A.M., S.D., and M.G. wrote the manuscript; all authors read and commented on the manuscript.

We declare no competing interests.

REFERENCES

1. Franck J, Arafah K, Elayed M, Bonnel D, Vergara D, Jacquet A, Vinatier D, Wisztorski M, Day R, Fournier I, Salzet M. 2009. MALDI imaging mass spectrometry. Mol Cell Proteomics 8:2023–2033. https://doi.org/10.1074/mcp.R800016-MCP200.
2. Fournier P-E, Drancourt M, Colson P, Rolain J-M, Scola BL, Raoult D. 2013. Modern clinical microbiology: new challenges and solutions. Nat Rev Microbiol 11:574–585. https://doi.org/10.1038/nrmicro3068.
3. Goff DA, Jankowski C, Tenover FC. 2012. Using rapid diagnostic tests to optimize antimicrobial selection in antimicrobial stewardship programs. Pharmacotherapy 32:677–687. https://doi.org/10.1002/j.1875-9114.2012.01137.x.
4. Steward CD, Raney PM, Morrell AK, Williams PP, McDougal LK, Jevitt L, McGowan JE, Jr, Tenover FC. 2005. Testing for induction of clindamycin resistance in erythromycin-resistant isolates of *Staphylococcus aureus*. J Clin Microbiol 43:1716–1721. https://doi.org/10.1128/JCM.43.4.1716-1721.2005.
5. Horvat RT. 2010. Review of antibiogram preparation and susceptibility testing systems. Hosp Pharm 45:6–S9. https://doi.org/10.1310/hpj4511-s6.
6. Cosgrove SE. 2006. The relationship between antimicrobial resistance and patient outcomes: mortality, length of hospital stay, and health care costs. Clin Infect Dis 42:S82–S89. https://doi.org/10.1086/499406.
7. Seale AC, Gordon NC, Islam J, Peacock SJ, Scott JAG. 2017. AMR Surveillance in low and middle-income settings - a roadmap for participation in the Global Antimicrobial Surveillance System (GLASS). Wellcome Open Res 2:92. https://doi.org/10.12688/wellcomeopenres.12527.1.
8. Safavieh M, Pandya HJ, Venkataraman M, Thirumalaraju P, Kanakasabapathy MK, Singh A, Prabhakar D, Chug MK, Shafiee H. 2017. Rapid real-time antimicrobial susceptibility testing with electrical sensing on plastic microchips with printed electrodes. ACS Appl Mater Interfaces 9:12832–12840. https://doi.org/10.1021/acsami.6b16571.
9. Syal K, Shen S, Yang Y, Wang S, Haydel SE, Tao N. 2017. Rapid antibiotic susceptibility testing of uropathogenic *E. coli* by tracking submicron scale motion of single bacterial cells. ACS Sens 2:1231–1239. https://doi.org/10.1021/acssensors.7b00392.
10. Liu C-Y, Han Y-Y, Shih P-H, Lian W-N, Wang H-H, Lin C-H, Hsueh P-R, Wang J-K, Wang Y-L. 2016. Rapid bacterial antibiotic susceptibility test based on simple surface-enhanced Raman spectroscopic biomarkers. Sci Rep 6:23375. https://doi.org/10.1038/srep23375.
11. Syal K, Iriya R, Yang Y, Yu H, Wang S, Haydel SE, Chen H-Y, Tao N. 2016. Antimicrobial susceptibility test with plasmonic imaging and tracking of single bacterial motions on nanometer scale. ACS Nano 10:845–852. https://doi.org/10.1021/acsnano.5b05944.
12. Schubert S, Kostrzewa M. 2015. Chapter 14. MALDI-TOF mass spectrometry in the clinical microbiology laboratory; beyond identification. Methods Microbiol 42:501–524. https://doi.org/10.1016/bs.mim.2015.04.004.
13. Pulido MR, García-Quintanilla M, Martín-Peña R, Cisneros JM, McConnell MJ. 2013. Progress on the development of rapid methods for antimicrobial susceptibility testing. J Antimicrob Chemother 68:2710–2717. https://doi.org/10.1093/jac/dkt253.
14. Didelot X, Bowden R, Wilson DJ, Peto TE, Crook DW. 2012. Transforming clinical microbiology with bacterial genome sequencing. Nat Rev Genet 13:601–612. https://doi.org/10.1038/nrg3226.
15. Dinarelli S, Girasole M, Kasas S, Longo G. 2017. Nanotools and molecular techniques to rapidly identify and fight bacterial infections. J Microbiol Methods 138:72–81. https://doi.org/10.1016/j.mimet.2016.01.005.
16. Mokrousov I, Chernyaeva E, Vyazovaya A, Sinkov V, Zhuravlev V, Narvskaya O. 2016. Next-generation sequencing of *Mycobacterium tuberculosis*. Emerg Infect Dis 22:1127–1129. https://doi.org/10.3201/eid2206.152051.
17. Mittman SA, Huard RC, Della-Latta P, Whittier S. 2009. Comparison of BD Phoenix to Vitek 2, MicroScan MICroSTREP, and Etest for antimicrobial susceptibility testing of *Streptococcus pneumoniae*. J Clin Microbiol 47:3557–3561. https://doi.org/10.1128/JCM.01137-09.
18. Rhoads S, Marinelli L, Imperatrice CA, Nachamkin I. 1995. Comparison of MicroScan WalkAway system and Vitek system for identification of gram-negative bacteria. J Clin Microbiol 33:3044–3046.
19. Boisen A, Dohn S, Keller SS, Schmid S, Tenje M. 2011. Cantilever-like micromechanical sensors. Rep Prog Phys 74:036101. https://doi.org/10.1088/0034-4885/74/3/036101.
20. Domínguez CM, Kosaka PM, Sotillo A, Mingorance J, Tamayo J, Calleja M. 2015. Label-free DNA-based detection of *Mycobacterium tuberculosis* and rifampicin resistance through hydration induced stress in microcantilevers. Anal Chem 87:1494–1498. https://doi.org/10.1021/ac504523f.
21. Etayash H, Khan MF, Kaur K, Thundat T. 2016. Microfluidic cantilever detects bacteria and measures their susceptibility to antibiotics in small confined volumes. Nat Commun 7:12947. https://doi.org/10.1038/ncomms12947.
22. Pelling AE, Sehati S, Gralla EB, Valentine JS, Gimzewski JK. 2004. Local nanomechanical motion of the cell wall of *Saccharomyces cerevisiae*. Science 305:1147–1150. https://doi.org/10.1126/science.1097640.
23. Radmacher M, Fritz M, Hansma HG, Hansma PK. 1994. Direct observation of enzyme-activity with the atomic-force microscope. Science 265:1577–1579. https://doi.org/10.1126/science.8079171.
24. Schneider SW, Egan ME, Jena BP, Guggino WB, Oberleithner H, Geibel JP. 1999. Continuous detection of extracellular ATP on living cells by using atomic force microscopy. Proc Natl Acad Sci U S A 96:12180–12185. https://doi.org/10.1073/pnas.96.21.12180.
25. Braun T, Ghatkesar MK, Backmann N, Grange W, Boulanger P, Letellier L, Lang H-P, Bietsch A, Gerber C, Hegner M. 2009. Quantitative time-resolved measurement of membrane protein-ligand interactions using microcantilever array sensors. Nat Nanotechnol 4:179–185. https://doi.org/10.1038/nnano.2008.398.
26. Ndieyira JW, Watari M, Barrera AD, Zhou D, Vogtli M, Batchelor M, Cooper MA, Strunz T, Horton MA, Abell C, Rayment T, Aeppli G, McKendry RA. 2008. Nanomechanical detection of antibiotic mucopeptide binding in a model for superbug drug resistance. Nature Nanotech 3:691–696. https://doi.org/10.1038/nnano.2008.275.
27. Berger R, Delamarche E, Lang HP, Gerber C, Gimzewski JK, Meyer E, Guntherodt HJ. 1997. Surface stress in the self-assembly of alkanethiols on gold. Science 276:2021–2024. https://doi.org/10.1126/science.276.5321.2021.
28. Burg TP, Godin M, Knudsen SM, Shen W, Carlson G, Foster JS, Babcock K, Manalis SR. 2007. Weighing of biomolecules, single cells and single nanoparticles in fluid. Nature 446:1066–1069. https://doi.org/10.1038/nature05741.
29. Park K, Millet LJ, Kim N, Li H, Jin X, Popescu G, Aluru NR, Hsia KJ, Bashir R. 2010. Measurement of adherent cell mass and growth. Proc Natl Acad Sci U S A 107:20691–20696. https://doi.org/10.1073/pnas.1011365107.
30. Kasas S, Longo G, Alonso-Sarduy L, Dietler G. October 2011. Nanoscale motion detector. Swiss patent PCT/IB2011054553.
31. Longo G, Alonso Sarduy L, Rio LM, Bizzini A, Trampuz A, Notz J, Dietler G, Kasas S. 2013. Rapid detection of bacterial resistance to antibiotics using AFM cantilevers as nanomechanical sensors. Nature Nanotechnol 8:522–526. https://doi.org/10.1038/nnano.2013.120.
32. Kasas S, Ruggeri FS, Benadiba C, Maillard C, Stupar P, Tournu H, Dietler G, Longo G. 2015. Detecting nanoscale vibrations as signature of life. Proc Natl Acad Sci U S A 112:378–381. https://doi.org/10.1073/pnas.1415348112.
33. Alonso-Sarduy L, De Los Rios P, Benedetti F, Vobornik D, Dietler G, Kasas S, Longo G. 2014. Real-time monitoring of protein conformational changes using a nano-mechanical sensor. PLoS One 9:e103674. https://doi.org/10.1371/journal.pone.0103674.
34. Ruggeri FS, Mahul-Mellier A-L, Kasas S, Lashuel HA, Longo G, Dietler G. 2017. Amyloid single-cell cytotoxicity assays by nanomotion detection. Cell Death Discov 3:17053. https://doi.org/10.1038/cddiscovery.2017.53.
35. Lissandrello C, Inci F, Francom M, Paul MR, Demirci U, Ekinci KL. 2014. Nanomechanical motion of *Escherichia coli* adhered to a surface. Appl Phys Lett 105:113701. https://doi.org/10.1063/1.4895132.
36. Wu S, Liu X, Zhou X, Liang XM, Gao D, Liu H, Zhao G, Zhang Q, Wu X. 2016. Quantification of cell viability and rapid screening anti-cancer drug

utilizing nanomechanical fluctuation. Biosens Bioelectron 77:164–173. https://doi.org/10.1016/j.bios.2015.09.024.
37. Yang F, Riedel R, Del Pino P, Pelaz B, Said AH, Soliman M, Pinnapireddy SR, Feliu N, Parak WJ, Bakowsky U, Hampp N. 2017. Real-time, label-free monitoring of cell viability based on cell adhesion measurements with an atomic force microscope. J Nanobiotechnology 15:23. https://doi.org/10.1186/s12951-017-0256-7.
38. Villalba MI, Stupar P, Chomicki W, Bertacchi M, Dietler G, Arnal L, Vela ME, Yantorno O, Kasas S. 2018. Nanomotion detection method for testing antibiotic resistance and susceptibility of slow-growing bacteria. Small 14:1702671. https://doi.org/10.1002/smll.201702671.
39. Stupar P, Opota O, Longo G, Prod'hom G, Dietler G, Greub G, Kasas S. 2017. Nanomechanical sensor applied to blood culture pellets: a fast approach to determine the antibiotic susceptibility against agents of bloodstream infections. Clin Microbiol Infect 23:400–405. https://doi.org/10.1016/j.cmi.2016.12.028.
40. Beaussart A, El-Kirat-Chatel S, Herman P, Alsteens D, Mahillon J, Hols P, Dufrêne YF. 2013. Single-cell force spectroscopy of probiotic bacteria. Biophys J 104:1886–1892. https://doi.org/10.1016/j.bpj.2013.03.046.
41. Tortoli E. 2014. Microbiological features and clinical relevance of new species of the genus *Mycobacterium*. Clin Microbiol Rev 27:727–752. https://doi.org/10.1128/CMR.00035-14.
42. Zumla AI, Gillespie SH, Hoelscher M, Philips PP, Cole ST, Abubakar I, McHugh TD, Schito M, Maeurer M, Nunn AJ. 2014. New antituberculosis drugs, regimens, and adjunct therapies: needs, advances, and future prospects. Lancet Infect Dis 14:327–340. https://doi.org/10.1016/S1473-3099(13)70328-1.
43. Calvori C, Frontali L, Leoni L, Tecce G. 1965. Effect of rifamycin on protein synthesis. Nature 207:417. https://doi.org/10.1038/207417a0.
44. Marianelli C, Armas F, Boniotti MB, Mazzone P, Pacciarini ML, Di Marco Lo Presti V. 2015. Multiple drug-susceptibility screening in *Mycobacterium bovis*: new nucleotide polymorphisms in the *embB* gene among ethambutol susceptible strains. Int J Infect Dis 33:39–44. https://doi.org/10.1016/j.ijid.2014.12.043.
45. Kolibab K, Derrick SC, Morris SL. 2011. Sensitivity to isoniazid of *Mycobacterium bovis* BCG strains and BCG disseminated disease isolates. J Clin Microbiol 49:2380–2381. https://doi.org/10.1128/JCM.00648-11.
46. Rastogi N, Goh K, Berchel M, Bryskier A. 2000. Activity of rifapentine and its metabolite 25-*O*-desacetylrifapentine compared with rifampicin and rifabutin against *Mycobacterium tuberculosis*, *Mycobacterium africanum*, *Mycobacterium bovis* and *M. bovis* BCG. J Antimicrob Chemother 46:565–570. https://doi.org/10.1093/jac/46.4.565.
47. Aon MA, Roussel MR, Cortassa S, O'Rourke B, Murray DB, Beckmann M, Lloyd D. 2008. The scale-free dynamics of eukaryotic cells. PLoS One 3:e3624. https://doi.org/10.1371/journal.pone.0003624.
48. Lloyd D, Cortassa S, O'Rourke B, Aon MA. 2012. What yeast and cardiomyocytes share: ultradian oscillatory redox mechanisms of cellular coherence and survival. Integr Biol (Camb) 4:65–74. https://doi.org/10.1039/C1IB00124H.
49. Kruse K, Julicher F. 2005. Oscillations in cell biology. Curr Opin Cell Biol 17:20–26. https://doi.org/10.1016/j.ceb.2004.12.007.
50. Schembri MA, Christiansen G, Klemm P. 2001. FimH-mediated autoaggregation of *Escherichia coli*. Mol Microbiol 41:1419–1430. https://doi.org/10.1046/j.1365-2958.2001.02613.x.
51. Maurer FP, Bruderer VL, Castelberg C, Ritter C, Scherbakov D, Bloemberg GV, Bottger EC. 2015. Aminoglycoside-modifying enzymes determine the innate susceptibility to aminoglycoside antibiotics in rapidly growing mycobacteria. J Antimicrob Chemother 70:1412–1419. https://doi.org/10.1093/jac/dku550.
52. Pryjma M, Burian J, Kuchinski K, Thompson CJ. 2017. Antagonism between front-line antibiotics clarithromycin and amikacin in the treatment of *Mycobacterium abscessus* infections is mediated by the *whiB7* gene. Antimicrob Agents Chemother 61:e01353-17. https://doi.org/10.1128/AAC.01353-17.
53. WHO. 2017. Global tuberculosis report 2017. World Health Organization, Geneva, Switzerland. https://www.who.int/tb/publications/global_report/gtbr2017_main_text.pdf.
54. Ibrahim EH, Sherman G, Ward S, Fraser VJ, Kollef MH. 2000. The influence of inadequate antimicrobial treatment of bloodstream infections on patient outcomes in the ICU setting. Chest 118:146–155. https://doi.org/10.1378/chest.118.1.146.
55. Premanandh J, Samara BS, Mazen AN. 2015. Race against antimicrobial resistance requires coordinated action – an overview. Front Microbiol 6:1536. https://doi.org/10.3389/fmicb.2015.01536.
56. Imperi F, Leoni L, Visca P. 2014. Antivirulence activity of azithromycin in *Pseudomonas aeruginosa*. Front Microbiol 5:178. https://doi.org/10.3389/fmicb.2014.00178.
57. Rampioni G, Visca P, Leoni L, Imperi F. 2017. Drug repurposing for antivirulence therapy against opportunistic bacterial pathogens. Emerg Top Life Sci 2017:ETLS20160018. https://doi.org/10.1042/etls20160018.
58. Formentín P, Catalán Ú, Pol L, Fernández-Castillejo S, Solà R, Marsal LF. 2018. Collagen and fibronectin surface modification of nanoporous anodic alumina and macroporous silicon for endothelial cell cultures. J Biol Eng 12:21. https://doi.org/10.1186/s13036-018-0111-x.
59. Kim YH, Baek NS, Han YH, Chung MA, Jung SD. 2011. Enhancement of neuronal cell adhesion by covalent binding of poly-D-lysine. J Neurosci Methods 202:38–44. https://doi.org/10.1016/j.jneumeth.2011.08.036.
60. Lupoli F, Vannocci T, Longo G, Niccolai N, Pastore A. 2018. The role of oxidative stress in Friedreich's ataxia. FEBS Lett 592:718–727. https://doi.org/10.1002/1873-3468.12928.
61. Dinarelli S, Girasole M, Longo G. 2018. FC_analysis: a tool for investigating atomic force microscopy maps of force curves. BMC Bioinformatics 19:258. https://doi.org/10.1186/s12859-018-2265-4.
62. Aghayee S, Benadiba C, Notz J, Kasas S, Dietler G, Longo G. 2013. Combination of fluorescence microscopy and nanomotion detection to characterize bacteria. J Mol Recognit 26:590–595. https://doi.org/10.1002/jmr.2306.
63. Kasas S, Radotic K, Longo G, Saha B, Alonso-Sarduy L, Dietler G, Roduit C. 2013. A universal fluid cell for the imaging of biological specimens in the atomic force microscope. Microsc Res Tech 76:357–363. https://doi.org/10.1002/jemt.22174.